



## A Sulfobetaine Zwitterionic Polymer-Drug Conjugate for Multivalent Paclitaxel and Gemcitabine Co-Delivery

Journal:	<i>Biomaterials Science</i>
Manuscript ID	BM-ART-03-2021-000393.R1
Article Type:	Paper
Date Submitted by the Author:	11-May-2021
Complete List of Authors:	Sun, Haotian; University at Buffalo, Department of Chemical and Biological Engineering Yan, Lingyue; University at Buffalo, Department of Biomedical Engineering Zhang, Runsheng; University at Buffalo, Department of Chemical and Biological Engineering Lovell, Jonathan; University at Buffalo, Department of Biomedical Engineering Wu, Yun; University at Buffalo, Department of Biomedical Engineering Cheng, Chong; University at Buffalo, Department of Chemical and Biological Engineering

## ARTICLE

## A Sulfobetaine Zwitterionic Polymer-Drug Conjugate for Multivalent Paclitaxel and Gemcitabine Co-Delivery

Haotian Sun,<sup>†a</sup> Lingyue Yan,<sup>‡b</sup> Runsheng Zhang,<sup>a</sup> Jonathan F. Lovell,<sup>b</sup> Yun Wu,<sup>\*b</sup> and Chong Cheng<sup>\*a</sup>

Received 00th January 20xx,  
Accepted 00th January 20xx

DOI: 10.1039/x0xx00000x

A zwitterionic polymer-drug conjugate (ZPDC) strategy is developed for the co-delivery of paclitaxel (PTX) and gemcitabine (GEM) chemotherapeutics, as well as a near-infrared fluorescence imaging agent cyanine5.5 (Cy5.5). The well-defined ZPDC is synthesized by tandem azide-alkyne and thiol-ene click functionalization of a biodegradable acetylenyl/allyl-functionalized polylactide and zwitterionic character is conferred by sulfobetaine. It has a number-average molecular weight of 53.6 kDa, comprising 6.5% PTX and 17.7% GEM by weight. Cy5.5 moieties are readily introduced to the ZPDC *via* conjugation. In aqueous solutions, the ZPDC exhibits a hydrodynamic diameter of 46 nm. *In vitro* MIA PaCa-2 human pancreatic cancer cells show strong ZPDC cellular uptake and cytotoxicity. In mice, the ZPDC exhibits long blood circulation, effective tumor accumulation, biocompatibility, therapeutic effect, and integrated imaging capacity. Overall, this work illustrates that ZPDCs are promising systems for chemotherapy delivery and bioimaging applications.

### Introduction

The development of novel and transformative materials for biomedical applications is a central aspect of biomaterial research. With minimal long-term side effects and systemic toxicity, biodegradable polymers have been broadly utilized in biomedical fields.<sup>1-7</sup> For instance, aliphatic polyesters, such as poly(lactic acid) (PLA) and polycaprolactone (PCL), are important biodegradable polymers that have been approved by FDA for specific *in vivo* clinical applications.<sup>8-11</sup> However, typical biodegradable polymers are hydrophobic and lack functionalities, and there is a significant need to develop well-defined hydrophilic biodegradable polymers carrying special functionalities to enhance their biomedical applicability.<sup>12-15</sup> In particular, such water-soluble or water-dispersible functional biodegradable polymers can be promising biomaterials for therapeutic delivery via systemic circulation.

Poly(ethylene glycol) (PEG) is an important type of polymer with significant biomedical applications.<sup>16</sup> Specifically, as the gold standard of stealth polymers, PEG is the most used polymer in the field of polymer-based therapeutic delivery. There are a broad variety of PEGylated therapeutics currently on the market for the treatment of numerous kinds of diseases.<sup>17, 18</sup> PEGylation confers the attached therapeutics a

protective layer to increase circulation time and bioavailability by mitigating clearance mechanisms. Moreover, PEGylation can improve the stability of therapeutics and enhance aqueous solubility of hydrophobic drugs. However, there are also limitations in PEGylation. First, it can decrease bioactivity of therapeutics, especially for proteins.<sup>19</sup> Second, the apparent antigenicity of PEG, as indicated through pre-existing and study-induced PEG-specific antibodies in animal models and humans, can restrict the biomedical efficacy of PEGylated therapeutics and modulate pharmacokinetic properties.<sup>20, 21</sup> Third, because typically only chain-ends of PEG can be used for functionalization, the conjugates of PEG with small-molecule drugs suffer from low drug loading amounts, which may result in insufficient therapeutic effects. Therefore, there is a need to develop new polymers as improved alternatives of PEG.

Over the past decade, zwitterionic polymers (ZPs) have attracted significant interests due to their special properties and promising potentials for biomedical applications.<sup>22-26</sup> Because zwitterionic groups are superhydrophilic, ZPs generally are more hydrophilic than PEG and may exert improved protection and solubility enhancement to therapeutics. ZP-modified nanoparticles (NPs) exhibited excellent long-circulation abilities, often yielding half-lives even longer than the equivalent PEGylated NPs.<sup>27, 28</sup> Because ZP-specific antibodies are absent, ZPs would not induce unfavorable immune response.<sup>27-29</sup> Moreover, as reported by Jiang and co-workers,<sup>30</sup> ZP-conjugated proteins showed improved stability without compromising bioactivity or binding affinity. However, the ZPs that so far have been studied intensively are non-biodegradable. Because ZPs have more compact solution conformations than PEG, a large amount of ZP relative to PEG is required to reach the same hydrodynamic

<sup>a</sup> Department of Chemical and Biological Engineering, University at Buffalo, The State University of New York, Buffalo, NY 14260, USA. E-mail: ccheng8@buffalo.edu

<sup>b</sup> Department of Biomedical Engineering, University at Buffalo, The State University of New York, Buffalo, NY 14260, USA. E-mail: ywu32@buffalo.edu

<sup>†</sup> Electronic Supplementary Information (ESI) available. See DOI: 10.1039/x0xx00000x

<sup>‡</sup> These authors contributed equally.

volume for biomedical modification.<sup>30</sup> Thus, side effects and systemic toxicity resulted from polymer accumulation present potential health risks that limit non-biodegradable ZP-modified

limited to *in vitro* assessment.<sup>39</sup> Therefore, it is important to develop biodegradable ZP-based therapeutics for broad biomedical studies, in order to lay a solid foundation to

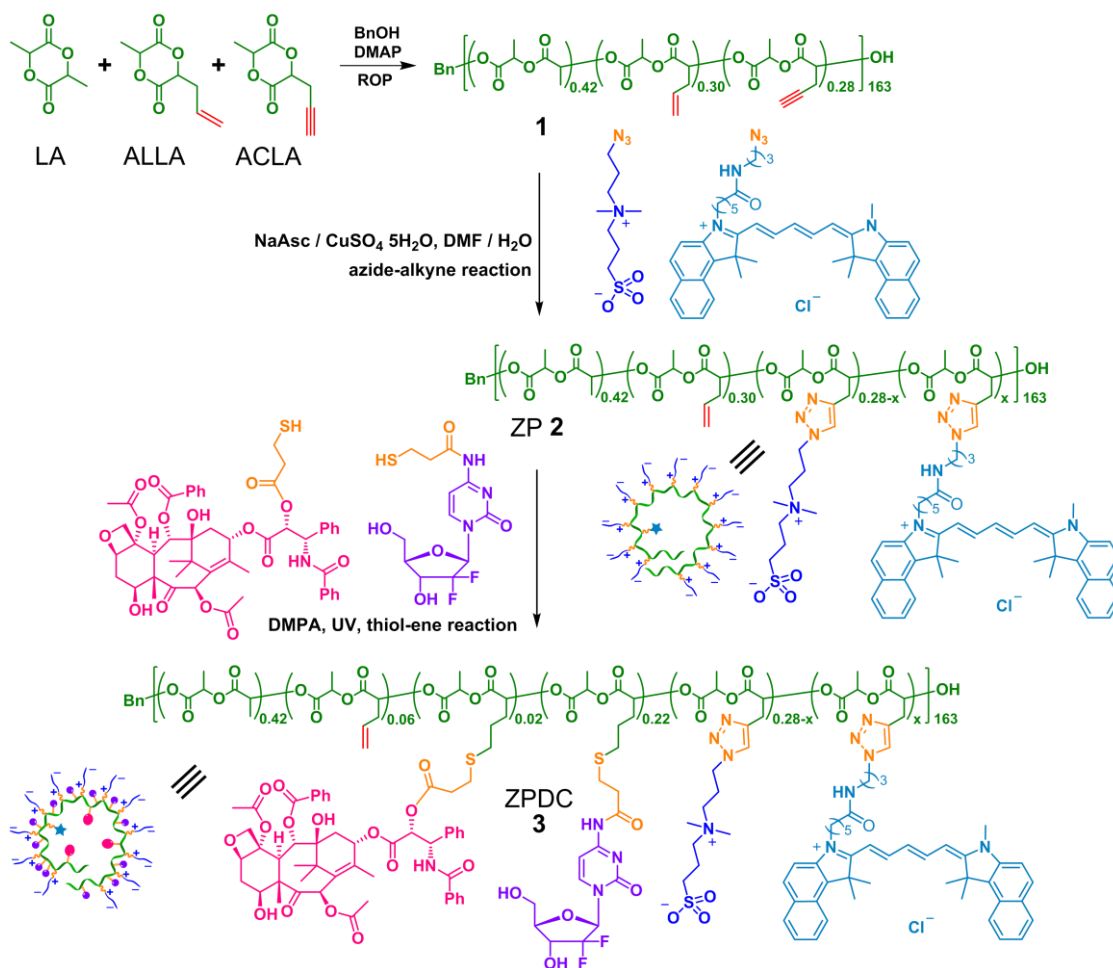


Fig. 1 Synthesis of ZPDC ( $x = 0$  without Cy5.5-labelling, and 0.01 with Cy5.5-labelling).

therapeutics for *in vivo* clinical applications.

Because the design of complex polymeric biomaterials with integrated non-biodegradable ZP blocks and degradable polymer blocks can only partly address the concerns, the development of ZPs with all biodegradable segments has attracted increasing interest in the past decade. Poly(amino acid)s or modified chitosan, with opposite charges carried by different monomer units have been reported.<sup>31-34</sup> Specifically, the solid phase synthesis of zwitterionic peptides demonstrated by Chen et al. can have precisely controlled alternating sequence of amino acid units carrying opposite charges.<sup>31</sup> Recently, Wu and co-workers reported polyacetal-based zwitterionic dendrimers that show pH-responsive degradation behavior and can be used for drug encapsulation and delivery.<sup>35</sup> Other examples of biodegradable ZPs with well-defined structures are prepared by side-chain functionalization of biodegradable precursor polymers.<sup>36-39</sup> Based on the synthesis and property studies of biodegradable ZPs, the conjugation of biodegradable ZPs with therapeutics has been investigated, but the corresponding biomedical studies were

transform these novel therapeutics to *in vivo* clinical applications.

The objective of this work is to develop functional sulfobetaine (SB)-containing zwitterionic PLA as a versatile platform for conjugating with multiple therapeutics, and to reveal biomedical relevant merits of the resulting ZP-drug conjugate (ZPDC). Owing to the robust, efficient, and orthogonal nature of click reactions, tandem click reactions were adopted in the synthesis (Fig. 1).<sup>40</sup> Because the combination therapy of paclitaxel (PTX) with gemcitabine (GEM) has been approved by FDA for the clinical treatment of pancreatic cancer,<sup>41</sup> ZPDC carrying both PTX and GEM moieties was prepared and *in vitro* and *in vivo* models of pancreatic cancer were used in biomedical studies.

## Experimental Section

### Materials

2,2-Dimethoxy-2-phenylacetophenone (DMPA; 99%) and sodium periodate (99%) were purchased from Acros Organics. Cyanine5.5 azide (Cy5.5-N<sub>3</sub>) was purchased from Lumiprobe Corporation. PTX (99%) was purchased from AvaChem Scientific. GEM (98+%) was purchased from Ark Pharm. Ruthenium dioxide (99.9%) was purchased from Pfaltz & Bauer. L-Ascorbic acid sodium salt (NaAsc), copper sulfate pentahydrate (CuSO<sub>4</sub>•5H<sub>2</sub>O), *N,N'*-dimethylformamide (DMF; HPLC grade), dichloromethane (DCM, HPLC grade), methanol (MeOH, HPLC grade), chloroform (CHCl<sub>3</sub>, HPLC grade), hexanes (HPLC grade), diethyl ether (HPLC grade), and acetonitrile (HPLC grade) were purchased from Fisher Scientific. DMF and DCM were dried by distillation over CaH<sub>2</sub>. Acetylenyl-functionalized lactide (ACLA), allyl-functionalized lactide (ALLA), and copolymer **1** were freshly prepared following the methods reported in our previous publications.<sup>42, 43</sup> Thiol-functionalized PTX (PTX-SH) and GEM (GEM-SH) were prepared according to approaches reported in the literature, respectively.<sup>44, 45</sup>

### Synthesis of PLA-g-SB (ZP 2)

To a 10-mL reaction flask were added with **1** (300 mg), 6.0 mL of DMF, SB-N<sub>3</sub> (142 mg), and NaAsc (10.2 mg) were added with 0.50 mL of water. The flask was tightly sealed and degassed with N<sub>2</sub>. Then an aqueous solution of CuSO<sub>4</sub>•5H<sub>2</sub>O (6.40 mg in 0.25 mL of water) was added slowly using a syringe. The overall feed ratio was [acetylenyl group of **1**]<sub>0</sub>: [SB-N<sub>3</sub>]<sub>0</sub>: [CuSO<sub>4</sub>•5H<sub>2</sub>O]<sub>0</sub>: [NaAsc]<sub>0</sub> = 1.0:1.1:0.05:0.10. Three cycles of freeze-pump-thaw were performed to remove oxygen from the reaction system. The reaction mixture was stirred for 20 h at room temperature. The crude product was dialyzed against DCM:MeOH (v/v = 2:1), to remove unreacted SB-N<sub>3</sub>. The solution was filtrated and completely dried to give **2** (308 mg, 71.7% yield) as a white solid.  $M_n^{\text{NMR}} = 37.1$  kDa.

Cy5.5-labelled ZP **2**, PLA-g-SB/Cy5.5, was also synthesized using the same approach, except that 1.8 mol% of SB-N<sub>3</sub> was replaced by Cy5.5-N<sub>3</sub> in the azide-alkyne reaction.

### Synthesis of PLA-g-SB/PTX/GEM (ZPDC 3)

In a 10-mL reaction flask, **2** (227 mg), PTX-SH (34.8 mg, containing 31.6 mg of PTX), GEM-SH (104.4 mg, containing 78.2 mg of GEM), and DMPA (39.0 mg) were dissolved with 10.5 mL of the mixed solvent of CHCl<sub>3</sub> and MeOH (v/v, 2:1). The overall feed ratio was [allyl group of **2**]<sub>0</sub>: [PTX-SH]<sub>0</sub>: [GEM-SH]<sub>0</sub>: [DMPA]<sub>0</sub> = 1:0.12:0.98:0.50. Three freeze-pump-thaw cycles were conducted to remove oxygen from the reaction system. Then the mixture was irradiated under UV light ( $\lambda_{\text{max}} = 365$  nm, 90 min) at room temperature. The crude product was firstly dialyzed against a mixture of DCM and MeOH (v/v, 2:1) for 5 days, then precipitated in 75 mL of hexane using centrifuge. The precipitate was washed with DCM in ultrasonic bath to further remove possible trace amounts of organic impurities. The product was finally precipitated in 75 mL of cold diethyl ether to give **3** (237 mg, 67.1% yield) as a white solid after drying under vacuum.  $M_n^{\text{NMR}} = 53.6$  kDa.

Cy5.5-labelled ZPDC **3**, i.e. PLA-g-SB/Cy5.5/PTX/GEM, was also synthesized using the same approach, except that Cy5.5-labelled ZP **2** used in the thiol-ene reaction.

### Characterization

<sup>1</sup>H NMR spectra of ZP **2** and ZPDC **3** were recorded using a 500 MHz Varian INOVA-500 spectrometer at 25 °C, using a mixture of CDCl<sub>3</sub>/CD<sub>3</sub>OD (v/v, 1:1) as the solvent. Proton 2D diffusion-ordered spectroscopy (DOSY) data on the ZPDC **3**, PTX-SH, GEM-SH, PTX, GEM in CDCl<sub>3</sub>/CD<sub>3</sub>OD (v/v, 1:1) were acquired on a Varian INOVA NMR spectrometer operating at 500 MHz at room temperature, using the vendor supplied bipolar pulse pair stimulated echo (Dbppste) pulse sequence. The gradient was varied nonlinearly from 2.3278 to 58.2176 gauss/cm (15 steps), using a 120 ms diffusion delay and a diffusion gradient length of 2.0 ms; 64 transients were collected for each of the 15 incremented gradient values, with a one-second relaxation delay. The data were analyzed using MestReNova, and shown after Bayesian transformation.

Dynamic light scattering (DLS) was used to determine hydrodynamic diameter ( $D_h$ ), size distribution and zeta potential of self-assembled ZPDC **3**. Measurements of  $D_h$  and size distribution were performed on Zetasizer Nano ZS/ZS90 (Malvern Instruments Ltd.) with a 4 mM 633 nm HeNe laser as the light source at 25 °C. ZPDC **3** sample was simply dispersed in water (1 mg/mL) for measurements.

Transmission electron microscopy (TEM) was used to visualize self-assembled ZPDC **3**. The TEM images were obtained with a JEOL 2010 microscope. Dilute solutions (7  $\mu$ L each) of ZPDC **3** in water (~0.1 mg/mL) were dip coated onto the 400 mesh carbon-coated copper grids. After overnight drying under vacuum, the samples were stained for 3 h by a freshly prepared 0.5% solution of ruthenium tetroxide (RuO<sub>4</sub>). The staining agent was prepared by dissolving sodium periodate in water at first, followed by the addition of ruthenium dioxide. The reaction mixture was stirred for 1 h before use.

### In Vitro Cytotoxicity

The *in vitro* cytotoxicity was evaluated based on the cell viability of MIA PaCa-2 cells at 24 and 72 h after the treatment of ZPDC **3** at different concentrations. MIA PaCa-2 cells were first seeded in 96 well plates (Greiner Bio-one, 655180) at a seeding density of  $1 \times 10^4$  cells/well in 100  $\mu$ L cell culture medium. The cells were incubated at 37 °C overnight. The solutions of ZP **2**, the mixture of free PTX and GEM (PTX+GEM), and ZPDC **3** were prepared separately in cell culture medium while maintaining consistent PTX/GEM concentrations. Specifically, PTX+GEM samples were prepared at PTX concentration of 0.001, 0.05, 0.1, 0.5, 1, 5  $\mu$ g/mL and at GEM concentration of 0.002, 0.12, 0.24, 1.2, 2.4, 12  $\mu$ g/mL. ZPDC **3** had the same PTX/GEM concentrations as PTX+GEM, while ZP **2** and ZPDC **3** had the same polymer concentrations. PBS treated cells were used as the control group. At 24 and 72 h post treatment, cell viability was measured by using

AlamarBlue (Invitrogen, DAL1025) following the instruction of manufacturer. Briefly, 10% (v/v) AlamarBlue solution was prepared in cell culture medium and then added to cells and incubated with cells at 37 °C for 3 h, protected from light. A TECAN microplate reader (San Jose, CA) was used to measure the fluorescence at an excitation and emission wavelength of 560 and 590 nm, respectively. The cell viability of treated groups was normalized to the cell viability of the control group.

#### ***In Vitro* Cellular Uptake**

MIA PaCa-2 cells (CRL-1420, American Type Culture Collection, Manassas, Virginia) were seeded at  $2 \times 10^5$  cells per well in 6 well plates. After incubation at 37 °C overnight, the cells were treated with Cy5.5-N<sub>3</sub> and Cy5.5-labelled ZPDC **3** at a Cy5.5 concentration of 0.2 µg/mL. PBS treated cells were used as the negative control. The cells were harvested 24 h post treatment, and preserved in 4% paraformaldehyde (Acros, 41678-5000) at 4 °C for further analysis by flow cytometry and confocal microscopy.

For cell flow cytometry, 10,000 events were measured for each sample by a BD Fortessa flow cytometer (BD bioscience, San Jose, CA) in the APC channel ( $\lambda_{\text{ex}} = 640$  nm and  $\lambda_{\text{em}} = 660$  nm). There are three groups in total: PBS control, Cy5.5-N<sub>3</sub> and Cy5.5-labelled ZPDC **3** treated groups. Each group had three replicates. The mean fluorescence intensity  $\pm$  standard deviation of Cy5.5 were reported to evaluate the cellular uptake of Cy5.5-labelled ZPDC **3**. For confocal microscopy imaging, the cell nuclei were stained by DAPI (Sigma Aldrich, D8417). After staining, the cells were fixed on glass slides and imaged by the LSM 710 confocal microscope (ZEISS, Dublin, CA). The DAPI channel ( $\lambda_{\text{ex}} = 405$  nm and  $\lambda_{\text{em}} = 460$  nm) and Cy5 channel ( $\lambda_{\text{ex}} = 640$  nm and  $\lambda_{\text{em}} = 660$  nm) were chosen to elucidate cell nuclei and uptake of Cy5.5-labelled ZPDC **3**, respectively.

#### ***In Vivo* Biodistribution**

All animal procedures were performed in accordance with Animal Welfare Regulations (CFR, Title 9, Chapter 1, Subchapter A, Parts 1, 2 and 3) and the Guide for the Care and Use of Laboratory Animals and approved by the Institutional Animal Care and Use Committee (IACUC) at University at Buffalo. The biodistribution of ZPDC **3** was investigated in human pancreatic tumor xenograft model. MIA PaCa-2 cells ( $5 \times 10^6$  cells) were subcutaneously injected at the right flanks of female athymic nude mice (6-week old, Charles River Laboratories). Tumor volume was calculated by the equation  $V = (L \times W^2)/2$ . When the tumor volume reached 100 mm<sup>3</sup>, the mice were injected with PBS control, Cy5.5-N<sub>3</sub> and Cy5.5-labelled ZPDC **3** by mouse tail vein at Cy5.5 dose of 1.5 mg/kg of body weight. Whole body fluorescence images before and at 5 min, 1 h, 4 h, 24 h after injection were taken by IVIS Lumina II *in vivo* imaging system (PerkinElmer, Waltham, MA). At 24 h after injection, mice were sacrificed to collect tumors and major organs (including brain, heart, liver, spleen, lung

and kidney). The fluorescence signals of Cy5.5 in tumors and major organs were measured by the IVIS Lumina II *in vivo* imaging system to determine the biodistribution of ZPDC **3**.

#### ***In Vivo* Therapeutic Effect Evaluation**

The *in vivo* antitumor efficacy was evaluated based on the tumor growth of human pancreatic tumor xenograft model. MIA PaCa-2 cells ( $5 \times 10^6$  cells) were subcutaneously injected at the right flanks of 6-week old female athymic nude mice. When the tumor volume reached 100 mm<sup>3</sup>, the mice were randomly assigned into 4 groups (n = 8). PBS control, ZPDC **2**, PTX+GEM, and ZPDC **3** were administered intravenously every 3 days for a total of 6 injections. PTX+GEM and ZPDC **3** were given to mice at PTX doses of 10 mg/kg body weight and GEM doses of 24 mg/kg body weight. Tumor volumes and body weights were measured every day. The average tumor volume of each group  $\pm$  standard deviation was reported. Mice were sacrificed 3 days after the last injection. Blood, tumors and major organs were collected for further analysis.

#### **Immunohistochemical Staining**

Tumors tissues were harvested and fixed in 10% buffered formalin phosphate (Fisher Chemical, SF100-4). Then, the fixed tissues were embedded in paraffin and sliced at 4 µm to mount on glass slides. The slides were deparaffinized, rehydrated to water and placed in pre-heated citrate pH 6 (Dako, S1699) for target retrieval. Then, 3% hydrogen peroxide methanol solution was used to quench the tissues. The quenched tissues were blocked with Serum Free (Dako, S3022) for 10 min and stained with primary antibodies against Ki67 (ThermoFisher, RM9106) and cleaved caspase 3 (Cell Signalling, 9661). The positive staining results were observed after incubation of the slides with Goat Anti-Rabbit (Vector, BA-1000). The sections were also counterstained in Richard Allen hematoxylin 2 (ThermoFisher, 7231). The images of these tissues were taken by the use of a 2.2.1 RT color CCD camera (Diagnostic Instruments/SPOT, USA) of a TS100 microscope (Nikon, Japan).

#### **Blood Chemistry Panel**

Mouse whole blood was collected from retro-orbital sinus in tubes coated with lithium heparin. The blood cells were removed by centrifuging at 4000 rpm for 5 min. The plasma was then sent for standard chemistry panel analysis using an Element DC Chemistry Analyzer (Heska, USA).

## **Results and discussion**

#### **Design and Synthesis of ZPDC**

A PLA backbone polymer was covalently linked with SB, PTX, and GEM in the structural design of ZPDC **3**. PLA was chosen as it is a well-known biodegradable polymer with verified hydrolytic degradability.<sup>2, 42</sup> Superhydrophilic zwitterionic SB was selected to conjugate with the PLA backbone via a non-cleavable triazole-based linkage to reduce the unfavorable

interactions of ZPDC with biomolecules under biological conditions.<sup>39</sup> Chemotherapeutic PTX and GEM moieties were designed to conjugate with the PLA backbone via hydrolysable ester-thioether and amide-thioether linkages, which can result in sustained drug release faster than the degradation of the PLA backbone.<sup>46</sup> In addition, Cy5.5, a near-infrared fluorescence imaging dye, was selected to covalently linked with the PLA backbone via a non-cleavable triazole-based linkage for the

proton at  $\sim 2.1$  ppm) indicated the consumption of all of the acetylenyl groups on copolymer **1**, and on average the presence of 44.6 SB moieties per molecule of **2**. Thus, ZP **2** had a  $M_n^{\text{NMR}}$  of 37.1 kDa, with 30.1 wt% of SB. In addition, the quantitative presence of  $-\text{CH}=\text{}$  proton from allyl groups at 5.87–5.67 ppm illustrated that allyl groups of **1** were intact under the azide-alkyne reaction conditions.

PTX/GEM-dually conjugated ZPDC **3** was prepared by UV-

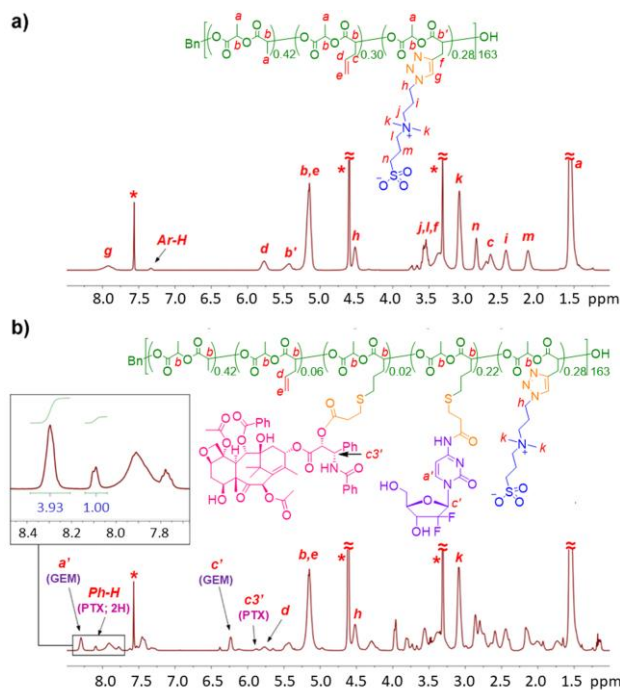


**Fig. 2** NMR Characterization of materials.  $^1\text{H}$  NMR spectra of a) ZP **2**, b) ZPDC **3** without Cy5.5 labelling in  $\text{CDCl}_3/\text{CD}_3\text{OD}$  (v/v, 1:1; \*: solvent resonances).

studies in which bioimaging was used.<sup>46</sup>

Using an acetylenyl/allyl-functionalized PLA **1** as the precursor polymer, PLA-based functional ZP **2** and ZPDC **3** were prepared through a click functionalization strategy (Fig. 1). Precursor **1** ( $M_n^{\text{NMR}} = 26.0$  kDa;  $M_n^{\text{GPC}} = 30.9$  kDa,  $M_w/M_n^{\text{GPC}} = 1.21$ , relative to linear polystyrene), as a copolymer of lactide (LA), acetylenyl-functionalized LA (ACLA) and allyl-functionalized LA (ALLA), has a structural formula of poly(LA<sub>0.42</sub>-co-ALLA<sub>0.30</sub>-co-ACLA<sub>0.28</sub>)<sub>163</sub>. The synthesis and characterization of **1** has been described previously.<sup>46</sup>

SB/allyl-functionalized PLA-based ZP **2** was synthesized by copper(I)-catalyzed azide-alkyne cycloaddition (CuAAC) click reactions of presynthesized azide-functionalized SB (SB-N<sub>3</sub>) with **1**, using a conventional  $\text{CuSO}_4 \cdot 5\text{H}_2\text{O}$  / NaAsc catalytic system in a mixture of DMF and water (v/v = 8:1) at room temperature for 20 h ([acetylenyl group of **1**]<sub>0</sub>: [SB-N<sub>3</sub>]<sub>0</sub>: [CuSO<sub>4</sub>·5H<sub>2</sub>O]<sub>0</sub>: [NaAsc]<sub>0</sub> = 1.0:1.1:0.05:0.10).<sup>47</sup> The  $^1\text{H}$  NMR spectrum of ZP **2** was recorded using  $\text{CDCl}_3/\text{CD}_3\text{OD}$  (v/v, 1:1) as the solvent (Fig. 2a). Along with the quantitative presence of resonances from protons of SB moieties, the disappearance of resonances of characteristic protons of ACLA units (i.e.,  $\text{CHCH}_2\text{C}\equiv\text{CH}$  proton at  $\sim 2.9$  ppm and  $\text{CHCH}_2\text{C}\equiv\text{CH}$

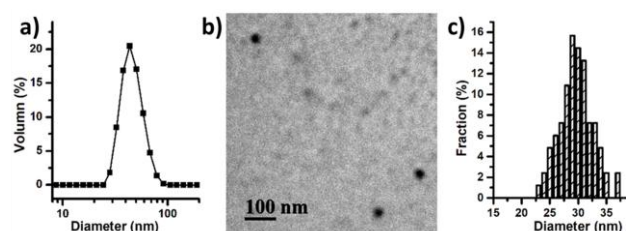


**Fig. 3** Size and morphology of ZPDC. a) Histograms of  $D_{h,v}$  of NPs of ZPLA **3** in aqueous solutions (1 mg/mL) measured by DLS; b) TEM image of NPs of ZPLA **3** from aqueous solutions (0.1 mg/mL); c) Histograms of diameter distribution of NPs of ZPLA **3** according to multiple TEM images ( $\sim 100$  particles counted, images not shown here). TEM samples were stained by  $\text{RuO}_4$ .

induced thiol-ene reaction of presynthesized thiol-functionalized PTX (PTX-SH) and GEM (GEM-SH) with ZP **2** in a mixed solvent of  $\text{CHCl}_3$  and MeOH (v/v, 2:1), with 2,2-dimethoxy-2-phenylacetophenone (DMPA) as photoinitiator ([allyl group of **2**]<sub>0</sub>: [PTX-SH]<sub>0</sub>: [GEM-SH]<sub>0</sub>: [DMPA]<sub>0</sub> = 1:0.12:0.98:0.50; weight ratio of PTX to GEM of 1:2.5).<sup>48, 49</sup> The reaction system was irradiated under UV light ( $\lambda_{\text{max}} = 365$  nm) for 90 min, yielding **3**.  $^1\text{H}$  NMR analysis of **3** in  $\text{CDCl}_3/\text{CD}_3\text{OD}$  (v/v, 1:1) revealed its composition (Fig. 2b). According to the resonance intensities of  $-\text{CH}=\text{}$  proton from the remaining allyl groups at  $\sim 5.8$  ppm, two aromatic protons from PTX at  $\sim 8.1$  ppm and  $>\text{NCH}=\text{}$  proton from GEM at  $\sim 8.3$  ppm, 80.4% of allyl groups of ZP **2** were consumed and the number ratio of conjugated units of PTX to GEM was 1.00:8.86 in the resulting ZPDC **3**. Thus, on average a molecule of ZPDC **3** had 4.1 PTX units and 35.9 GEM units, with the weight ratio of PTX to GEM of 1:2.4, which is in the range of PTX/GEM mass ratios (from 1:1 to 1:25) studied in the literature on PTX/GEM co-delivery.<sup>50-58</sup> Such  $^1\text{H}$  NMR results indicated that ZPDC **3** had a  $M_n^{\text{NMR}}$  of 53.6 kDa, with 6.5 wt% of PTX and 17.7 wt% of GEM. Noteworthy, both ZPDC **3** and its precursor ZP **2** could not be dissolved unimolecularly in common solvents for gel permeation chromatography (GPC), and therefore, their GPC analysis could not be performed.

To further demonstrate that the ZPDC **3** had well-defined structure without unreacted PTX-SH/GEM-SH and pre-released PTX/GEM, proton 2D DOSY NMR spectra of ZPDC **3**, PTX-SH, GEM-SH, PTX, GEM in  $\text{CDCl}_3/\text{CD}_3\text{OD}$  (v/v, 1:1) were acquired.<sup>59, 60</sup> The data were analyzed, and are shown after Bayesian transformation in Fig. S1. The different diffusion coefficients between ZPDC **3** and the other small molecules revealed that all of the PTX/GEM signals in spectrum of ZPDC **3** (Fig. S1a) are from conjugated PTX/GEM moieties.<sup>61</sup> In other words, ZPDC **3**

was pure, without being contaminated by free small molecule drugs, and the conjugation linkages between the PTX/GEM moieties and the ZP scaffold maintained stability under the

2 and ZPDC 3 (Fig. 1), except that a small portion (1.8 mol%) of SB-N<sub>3</sub> was replaced by Cy5.5-N<sub>3</sub> in the azide-alkyne reaction with functional PLA 1 ([acetylenyl group of 1]<sub>0</sub>:[SB-N<sub>3</sub>]<sub>0</sub>:[Cy5.5-N<sub>3</sub>]<sub>0</sub> = 1.0:1.08:0.02). Other than the presence of trace

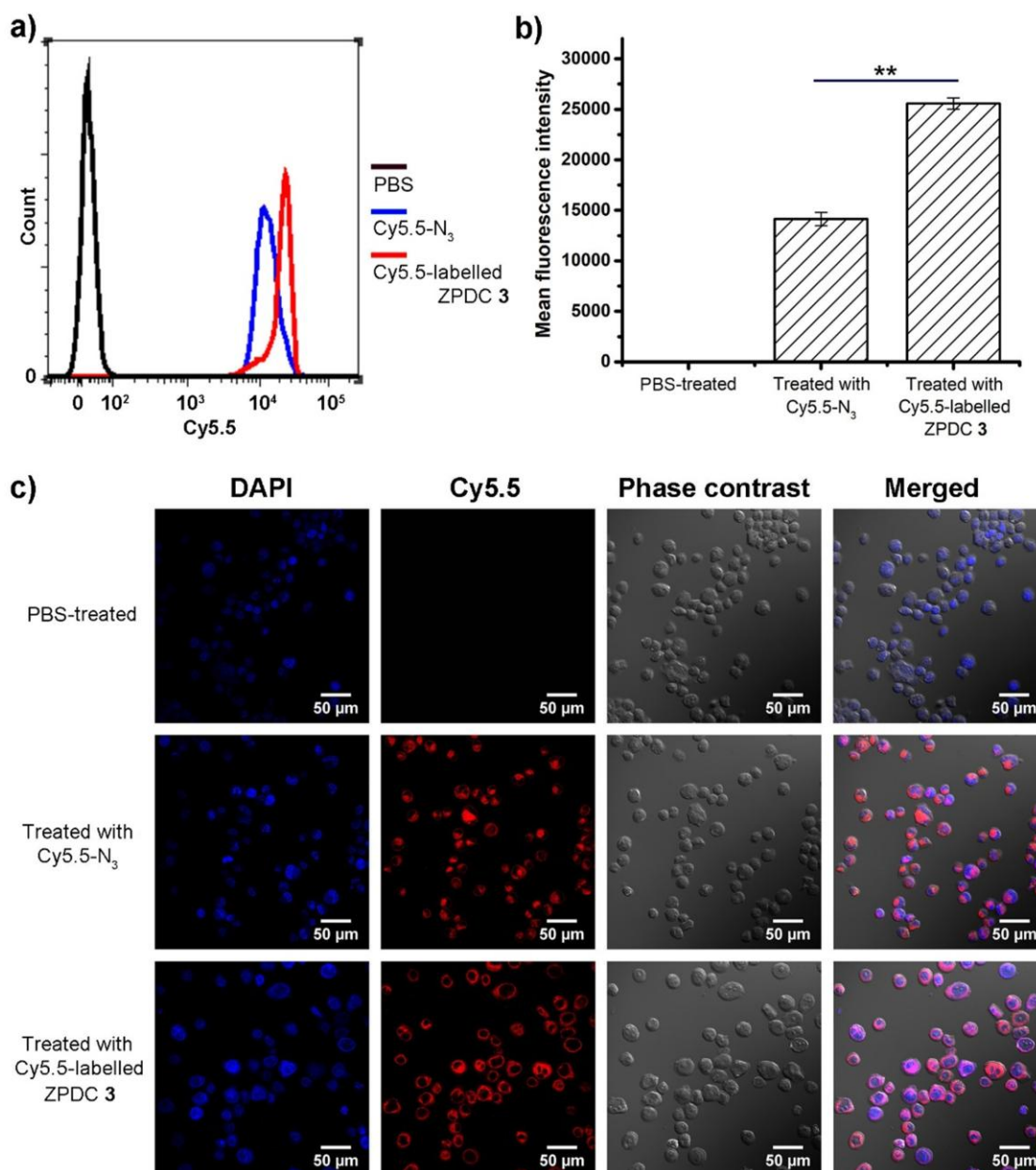


**Fig. 4** Cellular uptake of ZPDC. a) A representative flow cytometry data set, and b) mean fluorescence intensities of Cy5.5 in cells at 24 h post treatment with PBS control, free Cy5.5-N<sub>3</sub> and Cy5.5-labelled ZPDC 3. For each data, error bar represents standard deviation of three independent experiments. One-way ANOVA was used to assess the statistical significance of the data. \*\**p* < .01 was considered as statistically highly significant; c) confocal microscopy images of MIA Paca-2 cells at 24 h post treatment with free Cy5.5-N<sub>3</sub> and Cy5.5-labelled ZPDC 3. Cell nuclei were counterstained with DAPI.

NMR analytic conditions.

It should be noted that ZP 2 and ZPDC 3 can be readily conjugated with an optical imaging agent in either CuAAC or thiol-ene functionalization step. In this work, Cy5.5 was selected as the imaging agent, and Cy5.5-labelled ZP 2 and ZPDC 3 were prepared following the same approaches and conditions as those for the preparation of the non-labelled ZP

amounts of Cy5.5 (on average one Cy5.5 unit per molecule, according to UV-vis spectroscopy analysis), Cy5.5-labelled ZP 2 and ZPDC 3 were essentially identical with the non-labelled ones regarding structures and compositions as indicated by <sup>1</sup>H NMR analysis.

#### Nanostructure Characterization of ZPDC

With amphiphilic structure, ZPDC **3** assembled in aqueous solutions, and the resulting nanoparticles (NPs) were characterized by both DLS and TEM. DLS analysis showed that NPs of ZPDC **3** had a volume-average hydrodynamic diameter ( $D_{h,v}$ ) of  $45.6 \pm 2.1$  nm with a polydispersity (PDI) of 0.297 (Fig. 3a), with zeta potential of  $-5.0 \pm 0.5$  mV. TEM imaging revealed spherical morphology of NPs of ZPDC **3** on TEM grids, with number-average diameter ( $D_{av}$ ) of  $29.7 \pm 2.9$  nm (Fig. 3b-c). The  $D_{h,v}$  value of these NPs was larger than the  $D_{av}$  value, because  $D_{h,v}$  and  $D_{av}$  correspond to the solvated state and the dry state of the NPs, respectively.

### In Vitro Cellular Uptake Analysis

The uptake of Cy5.5-labelled ZPDC **3** in MIA PaCa-2 cancer cells was investigated using flow cytometry and confocal microscopy. Cells were treated with PBS control, free Cy5.5- $N_3$ , and Cy5.5-labelled ZPDC **3** at Cy5.5 concentration of 0.2  $\mu\text{g}/\text{mL}$ . The cells were harvested at 24 h post treatment. Flow

cytometry quantitatively analyzed the cellular uptake efficiency of free Cy5.5- $N_3$  and Cy5.5-labelled ZPDC **3** (Fig. 4a-b). The mean fluorescence intensity of Cy5.5 in cells treated by the Cy5.5-labelled ZPDC **3** was 1.8 times of those treated by

### In Vitro Cytotoxicity

*In vitro* cytotoxicity was examined to evaluate the therapeutic effects of ZPDC **3** in human pancreatic MIA PaCa-2 cells. PBS control, ZP **2** and the mixture of free PTX and GEM (PTX+GEM) were employed for comparison. ZPDC **3** and PTX+GEM had the same PTX/GEM concentrations ranging from 0.001/0.002  $\mu\text{g}/\text{mL}$  to 5/12  $\mu\text{g}/\text{mL}$ , while ZP **2** and ZPDC **3** had the same polymer concentrations. At 24 and 72 h post treatment, the cell viabilities were assessed. As shown in Fig. 5, ZP **2** did not induce noticeable cytotoxicity at all concentrations within 72 h, demonstrating the high biocompatibility of the polymer scaffold. At 24 h, ZPDC **3** showed better anti-cancer efficacy than PTX+GEM at PTX/GEM concentrations higher than 0.1/0.24  $\mu\text{g}/\text{mL}$ . At 72 h, similar toxicity behavior between free drug and ZPDC were also observed when PTX/GEM concentrations were higher than 0.1/0.24  $\mu\text{g}/\text{mL}$ .

### In Vivo Imaging and Biodistribution

Female athymic nude mice bearing subcutaneous MIA PaCa-2 pancreatic xenografts were used to investigate the biodistribution of ZPDC **3**.<sup>56, 62, 63</sup> When tumor volume reached 100  $\text{mm}^3$ , mice were randomly assigned to 3 groups. PBS control, Cy5.5- $N_3$ , and Cy5.5-labelled ZPDC **3** solutions were intravenously injected at Cy5.5 dose of 1.5  $\text{mg}/\text{kg}$  body weight, respectively. Before injection and at 5 min, 1 h, 4 h and 24 h post injection, *in vivo* fluorescence images of whole mice were recorded (dorsal side and ventral side). As shown in Fig. 6, the ZPDC **3** distributed across the mouse whole body immediately after injection, and remained in circulation even following 24 h, indicating that the ZPDC **3** had prolonged *in vivo* circulation time. The analysis of whole body fluorescence intensity of Cy5.5 showed that, relative to 5 min post injection of ZPDC **3**, there were 74.5%, 45.9% and 18.7% of ZPDC **3** circulating in the mice at 1, 4 and 24 h post treatment, respectively (Fig. S2). In contrast, Cy5.5- $N_3$  quickly accumulated in the liver and kidneys after IV injection, and little accumulation was observed in tumors. The prolonged circulation of ZPDC **3** is ascribed to the intrinsic properties of the nanoscopic ZP **2** scaffold with superhydrophilic SB groups to minimize unfavorable interactions with biomolecules and to slow down elimination. As supporting evidence, ZP **2** was given to healthy female nude mice with no tumors at Cy5.5 dose of 1.5  $\text{mg}/\text{kg}$  body weight and *in vivo* fluorescence images of whole mice showed that ZP **2** remained detectable for as long as 6 days (Fig. S3).

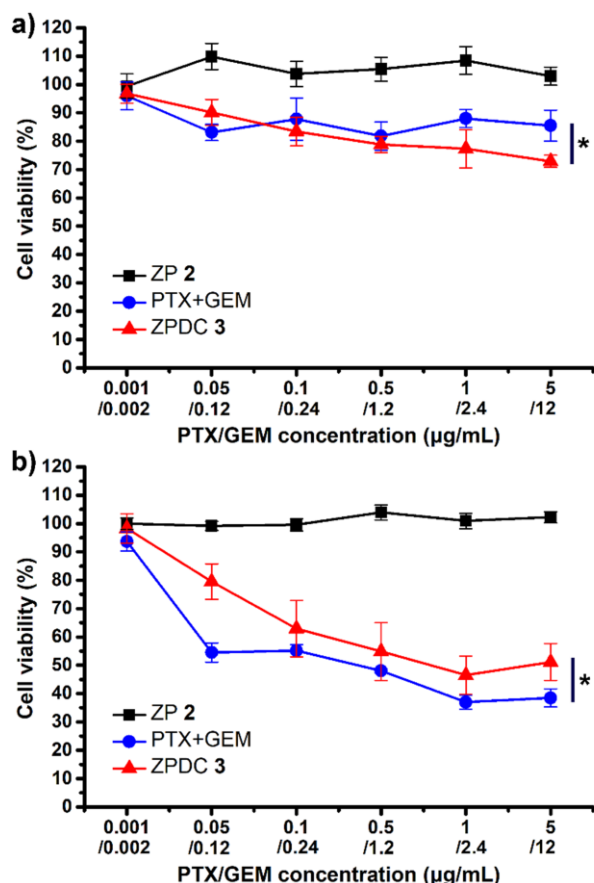


**Fig. 5** ZPDC Cytotoxicity. Cytotoxicity of ZP **2**, PTX+GEM, and ZPDC **3** in MIA PaCa-2 cells a) after 24 h treatment; b) after 72 h treatment. ZP **2** had the same polymer concentrations as ZPDC **3**. For each data, error bar represents standard deviation of three independent experiments. One-way ANOVA was used to assess the statistical significance of the data. \* $p < .05$  was considered as statistically significant.

cytometry quantitatively analyzed the cellular uptake efficiency of free Cy5.5- $N_3$  and Cy5.5-labelled ZPDC **3** (Fig. 4a-b). The mean fluorescence intensity of Cy5.5 in cells treated by the Cy5.5-labelled ZPDC **3** was 1.8 times of those treated by

*Ex vivo* fluorescence images of excised tumors and major organs at 24 h post injection are shown in Fig. 7. The mice treated with Cy5.5-labelled ZPDC 3 showed significant fluorescence signals in tumors, confirming the *in vivo* imaging results showing that ZPDC 3 effectively accumulated in MIA PaCa-2 tumors. No tumor accumulation of free Cy5.5-N<sub>3</sub> was observed. Fluorescence signal was also observed in the liver and kidney of mice treated by ZPDC 3, suggesting that the degradation residues of ZPDC 3 may have been excreted through metabolic routes in the liver and kidney.

### Therapeutic Efficacy

tumors grew to 100 mm<sup>3</sup>. PBS control, ZP 2, PTX+GEM, and ZPDC 3 were administrated intravenously at PTX doses of 10 mg/kg body weight and GEM doses of 24 mg/kg body weight every 3 days with a total of 6 injections. As shown in Fig. 8a, among all groups, ZPDC 3 showed the highest tumor growth inhibition effect. At the end of the study (day 18), the tumor volumes were an average of 948, 939, 637, and 378 mm<sup>3</sup> for vehicle, ZP 2, PTX+GEM, and ZPDC 3, respectively. As expected, no tumor inhibition was observed with ZP 2. ZPDC 3 showed a higher tumor inhibition rate (60.1%) than PTX+GEM (32.8%), demonstrating that ZPDC 3 provided a more effective anti-tumor efficacy than free PTX and GEM. Ki67 and cleaved

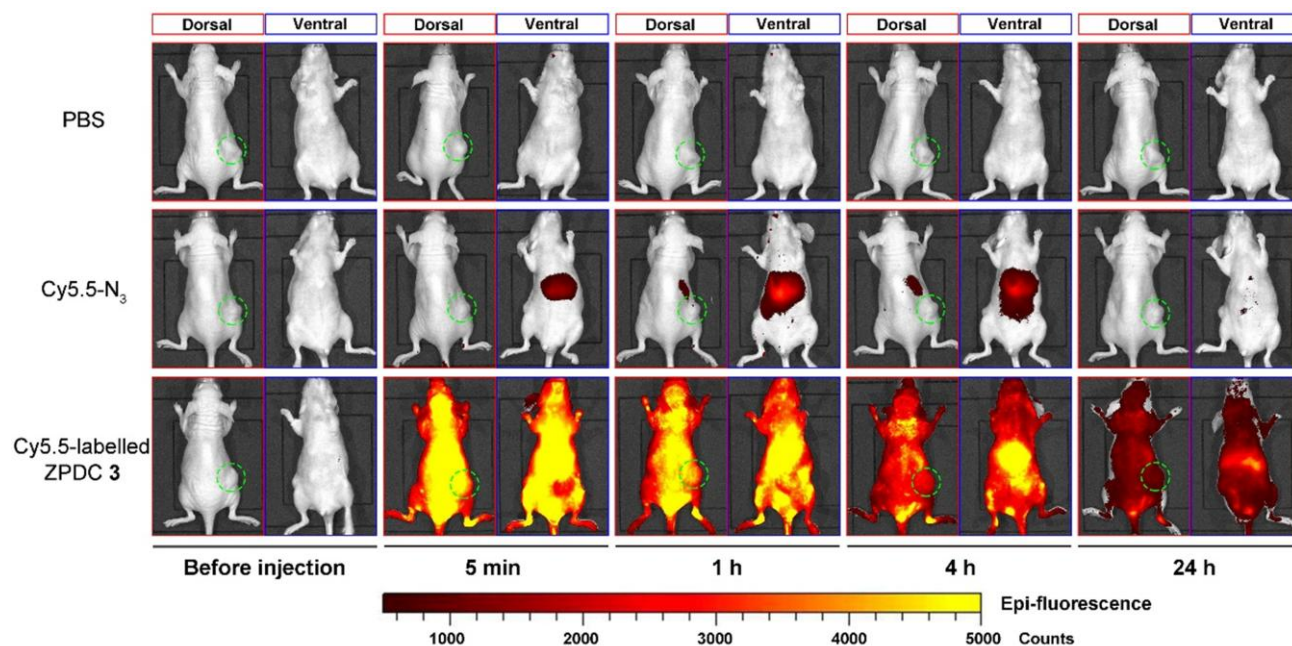


**Fig. 6** *In vivo* imaging. Representative whole body fluorescence images of mice (dorsal side and ventral side) before and at different time points (5 min, 1 h, 4 h, 24 h) post intravenous injection of PBS, Cy5.5-N<sub>3</sub>, Cy5.5-labelled ZPDC 3 at Cy5.5 dose of 1.5 mg/kg body weight. Tumors were circled in each dorsal side image.

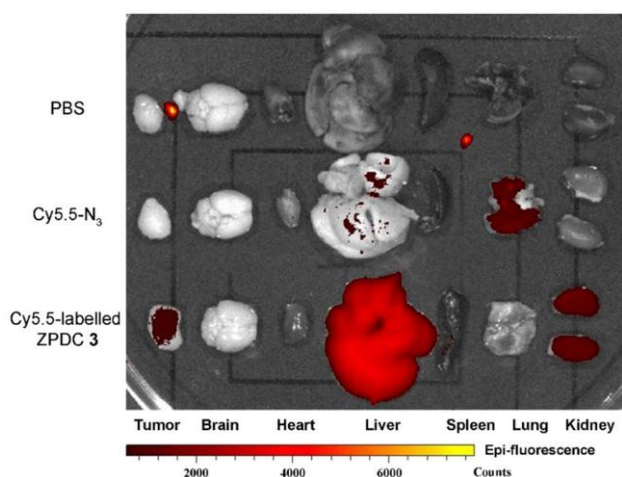


**Fig. 7** *Ex-vivo* organ imaging. Representative *ex vivo* fluorescence images of excised tumors and major organs at 24 h post intravenous injection of vehicle (PBS) control, Cy5.5-N<sub>3</sub>, Cy5.5-labelled ZPDC 3.

The *in vivo* antitumor efficacy of ZPDC 3 was evaluated with MIA PaCa-2 pancreatic tumor xenograft model. Female nude mice were randomly assigned into 4 groups ( $n = 8$ ) when

caspase 3 staining showed that tumors from ZPDC 3 group had lower proliferation and higher apoptosis than mice treated with ZP 2, PTX+GEM, and ZPDC 3 (Fig. 8b). These results demonstrated that ZPDC 3 successfully delivered PTX and GEM to tumors and significantly enhanced *in vivo* therapeutic effect.

The *in vivo* toxicity of ZP 2, PTX+GEM and ZPDC 3 were evaluated by monitoring the mouse body weight during the treatment and the blood panel analysis at the end of the study. As shown in Fig. 8c, no significant difference was observed in body weight among the mice treated with PBS, ZP 2, PTX+GEM and ZPDC 3. Compared with vehicle treated mice, the body weights were slightly increased by 4% for PTX+GEM treated mice, and 5% for ZPDC 3 treated mice.

At the end of the study, blood tests were performed to evaluate the kidney and liver functions of the mice (Table S1). No significant differences were observed in the levels of blood urea nitrogen (BUN), creatinine, alanine aminotransferase (ALT) and alkaline phosphatase (ALP), gamma-glutamyl transferase (GGT) and bilirubin among mice treated with PBS, ZP 2, PTX+GEM and ZPDC 3. Although the mice treated with ZP 2 and ZPDC 3 showed lower levels of calcium and cholesterol

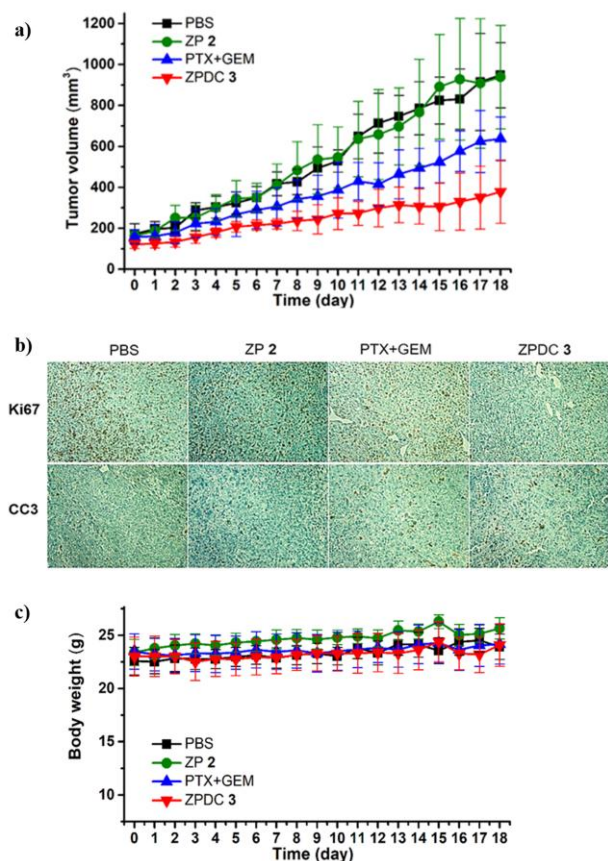


**Fig. 8** *In vivo* therapeutic effect and toxicity evaluation. Mice bearing subcutaneous MIA PaCa-2 xenografts were intravenously administered the indicated treatments every 3 days over the first 18 days of the study, which began when tumors reached 100 mm<sup>3</sup>. The PTX+GEM group and ZPDC 3 delivered 10 mg/kg PTX and 24 mg/kg GEM per injection. a) Changes in tumor volumes, b) Representative micrographs of Ki67 and cleaved caspase 3 immunohistochemistry staining of tumors, and c) changes in body weight during the treatment.

than those treated with PBS, the levels of calcium and cholesterol in these mice remained in normal range. These results suggest that the treatment with ZP 2, PTX+GEM and ZPDC 3 did not induce acute toxicity *in vivo* at the treatment doses.

## Conclusions

A novel multifunctional sulfobetaine-based ZPDC for co-delivery of hydrophobic PTX and hydrophilic GEM, with integrable tumor imaging function, was developed in this work. The ZPDC was synthesized by click multifunctionalization strategy via CuAAC and thiol-ene chemistries. The high purity of the ZPDC, with the absence of physically trapped small molecule drugs, was demonstrated by DOSY NMR analysis. The ZPDC had substantial loading amounts of PTX (6.5 wt%) and GEM (17.7 wt%), and long blood circulation. Moreover, significant *in vivo* therapeutic effect of the ZPDC was demonstrated in a human pancreatic tumor xenograft model. Blood chemistry panel analysis suggested no considerable side effects induced by the ZPDC. Thus, the multifunctional ZPDC

represents a promising design of integrated systems enabling co-delivery of multiple anticancer drugs of different hydrophilicity and tumor imaging.

## Conflicts of interest

There are no conflicts to declare.

## Acknowledgements

This work was supported by U. S. National Institutes of Health [R21 EBO24095-01] and U. S. National Science Foundation [DMR-1609914; CBET-1337860]. The authors thank the Magnetic Resonance Center (University at Buffalo), Dr. Dinesh Sukumaran and Elizabeth A. Shaw for the help to get access to DOSY NMR. The Zeiss LSM 710 confocal microscope at University at Buffalo North Campus Imaging Facility was funded by National Science Foundation Major Research Instrumentation Grant # DBI 0923133.

## Notes and references

- O. C. Farokhzad, J. Cheng, B. A. Teply, I. Sherifi, S. Jon, P. W. Kantoff, J. P. Richie and R. Langer, *Proc. Natl. Acad. Sci. U.S.A.*, 2006, **103**, 6315-6320.
- B. D. Ulery, L. S. Nair and C. T. Laurencin, *J. Polym. Sci., Part B: Polym. Phys.*, 2011, **49**, 832-864.
- H. Tian, Z. Tang, X. Zhuang, X. Chen and X. Jing, *Prog. Polym. Sci.*, 2012, **37**, 237-280.
- D. Shan, C. Ma and J. Yang, *Adv. Drug Deliv. Rev.*, 2019, **148**, 219-238.
- E. E. Leonhardt, N. Kang, M. A. Hamad, K. L. Wooley and M. Elsabahy, *Nat. Commun.*, 2019, **10**, 2307.
- L. Gao, J. Chen, W. Feng, Q. Song, J. Huo, L. Yu, N. Liu, T. Wang, P. Li and W. Huang, *Biomater. Sci.*, 2020, **8**, 6930-6945.
- M. A. Mohamed, A. Shahini, N. Rajabian, J. Caserto, A. M. A. El-Sokkary, M. A. Akl, S. T. Andreadis and C. Cheng, *Bioactive Mater.*, 2021, **6**, 2120-2133.
- Y. Ikada and H. Tsuji, *Macromol. Rapid Commun.*, 2000, **21**, 117-132.
- M. Hakkarainen, *Adv. Polym. Sci.*, 2002, **157**, 113-138.
- B. Gupta, N. Revagade and J. Hilborn, *Prog. Polym. Sci.*, 2007, **32**, 455-482.
- M. A. Woodruff and D. W. Hutmacher, *Prog. Polym. Sci.*, 2010, **35**, 1217-1256.
- R. M. Rasal, A. V. Janorkar and D. E. Hirt, *Prog. Polym. Sci.*, 2010, **35**, 338-356.
- C. K. Williams, *Chem. Soc. Rev.*, 2007, **36**, 1573-1580.
- Y. Yu, J. Zou and C. Cheng, *Polym. Chem.*, 2014, **5**, 5854-5872.
- Y. Lu, L. Yin, Y. Zhang, Z. Zhang, Y. Xu, R. Tong and J. Cheng, *ACS Macro Lett.*, 2012, **1**, 441-444.
- J. M. Harris, *Poly(ethylene glycol) Chemistry: Biotechnical and Biomedical Applications*, Springer, New York, 1992.
- J. M. Harris and R. B. Chess, *Nat. Rev. Drug Discovery*, 2003, **2**, 214-221.
- K. Knop, R. Hoogenboom, D. Fischer and U. S. Schubert, *Angew Chem. Int. Ed.*, 2010, **49**, 6288-6308.
- F. M. Veronese and A. Mero, *Biodrugs*, 2008, **22**, 315-329.

20. J. K. Armstrong, G. Hempel, S. Kolling, L. S. Chan, T. Fisher, H. J. Meiselman and G. Garratty, *Cancer*, 2007, **110**, 103-111.
21. M. S. Hershfield, N. J. Ganson, S. J. Kelly, E. L. Scarlett, D. A. Jagers and J. S. Sundry, *Arthritis Res. Ther.*, 2014, **16**, R63.
22. Z. G. Estephan, P. S. Schlenoff and J. B. Schlenoff, *Langmuir*, 2011, **27**, 6794-6800.
23. L. Mi and S. Jiang, *Angew. Chem. Int. Ed.*, 2014, **53**, 1746-1754.
24. X. Chen, S. McRae, S. Parelkar and T. Emrick, *Bioconjugate Chem.*, 2009, **20**, 2331-2341.
25. M.-C. Sin, S.-H. Chen and Y. Chang, *Polymer J.*, 2014, **46**, 436-443.
26. Z. Xiao, X. Zheng, Y. An, K. Wang, J. Zhang, H. He and J. Wu, *Biomater. Sci.*, 2021, **9**, 882-891.
27. W. Yang, S. Liu, T. Bai, A. J. Keefe, L. Zhang, J.-R. Ella-Menye, Y. Li and S. Jiang, *Nano Today*, 2014, **9**, 10-16.
28. S. Liang, Y. Liu, X. Jin, G. Liu, J. Wen, L. Zhang, J. Li, X. Yuan, I. S. Y. Chen, W. Chen, H. Wang, L. Shi, X. Zhu and Y. Lu, *Nano Res.*, 2016, **9**, 1022-1031.
29. L. Zhang, Z. Cao, T. Bai, L. Carr, J.-R. Ella-Menye, C. Irvin, B. D. Ratner and S. Jiang, *Nat. Biotech.*, 2013, **31**, 553-556.
30. A. J. Keefe and S. Y. Jiang, *Nat. Chem.*, 2012, **4**, 60-64.
31. S. F. Chen, Z. Q. Cao and S. Y. Jiang, *Biomaterials*, 2009, **30**, 5892-5896.
32. X. Wang, G. Wu, C. Lu, Y. Wang, Y. Fan, H. Gao and J. Ma, *Colloids Surf. B: Biointerfaces*, 2011, **86**, 237-241.
33. P. Xu, G. Bajaj, T. Shugg, W. G. V. Alstine and Y. Yeo, *Biomacromolecules*, 2010, **11**, 2352-2358.
34. S. Banskota, P. Yousefpour, N. Kirmani, X. Li and A. Chilkoti, *Biomaterials*, 2019, **192**, 475-485.
35. Y. Wang, D. Huang, X. Wang, F. Yang, H. Shen and D. Wu, *Biomater. Sci.*, 2019, **7**, 3238-3248.
36. S. Zhang, J. Zou, F. Zhang, M. Elsbahy, S. E. Felder, J. Zhu, D. J. Pochan and K. L. Wooley, *J. Am. Chem. Soc.*, 2012, **44**, 18467-18474.
37. E. M. Pelegri-O'Day, S. J. Paluck and H. D. Maynard, *J. Am. Chem. Soc.*, 2017, **139**, 1145-1154.
38. S.-H. Ye, Y. Chen, Z. Mao, X. Gu, V. Shankaraman, Y. Hong, V. Shanov and W. R. Wagner, *Langmuir*, 2018, **35**, 1421-1429.
39. H. Sun, M. Y. Z. Chang, W.-I. Cheng, Q. Wang, A. Comisso, M. Capeling, Y. Wu and C. Cheng, *Acta Biomater.*, 2017, **64**, 290-300.
40. R. K. Iha, K. L. Wooley, A. M. Nystrom, D. J. Burke, M. J. Kade and C. J. Hawker, *Chem. Rev.*, 2009, **109**, 5620-5686.
41. F. De Vita, J. Ventriglia, A. Febbraro, M. M. Laterza, A. Fabozzi, B. Savastano, A. Petrillo, A. Diana, G. Giordano, T. Troiani, G. Conzo, G. Galizia, F. Ciardiello and M. Orditura, *Bmc Cancer*, 2016, **16**.
42. Y. Yu, J. Zou, L. Yu, W. Jo, Y. K. Li, W. C. Law and C. Cheng, *Macromolecules*, 2011, **44**, 4793-4800.
43. J. Zou, C. C. Hew, E. Themistou, Y. K. Li, C. K. Chen, P. Alexandridis and C. Cheng, *Adv. Mater.*, 2011, **23**, 4274-4277.
44. J. Zou, F. W. Zhang, S. Y. Zhang, S. F. Pollack, M. Elsbahy, J. W. Fan and K. L. Wooley, *Adv. Healthc. Mater.*, 2014, **3**, 441-448.
45. M. Dasari, A. P. Acharya, D. Kim, S. Lee, S. Lee, J. Rhea, R. Molinaro and N. Murthy, *Bioconjugate Chem.*, 2013, **24**, 4-8.
46. H. Sun, L. Yan, M. Y. Z. Chang, K. A. Carter, R. Zhang, L. Slyker, J. F. Lovell, Y. Wu and C. Cheng, *Nanoscale Adv.*, 2019, **1**, 2761-2771.
47. H. C. Kolb, M. G. Finn and K. B. Sharpless, *Angew. Chem. Int. Ed.*, 2001, **40**, 2004-2021.
48. C. E. Hoyle and C. N. Bowman, *Angew. Chem. Int. Ed.*, 2010, **49**, 1540-1573.
49. L. M. Campos, K. L. Killops, R. Sakai, J. M. J. Paulusse, D. Damiron, E. Drockenmuller, B. W. Messmore and C. J. Hawker, *Macromolecules*, 2008, **41**, 7063-7070.
50. M. Lei, S. Sha, X. Wang, J. Wang, X. Du, H. Miao, H. Zhou, E. Bai, J. Shi and Y. Zhu, *RSC Adv.*, 2019, **9**, 5512-5520.
51. Y. Di, Y. Gao, X. Gai, D. Wang, Y. Wang, X. Yang, D. Zhang, W. Pan and X. Yang, *RSC Adv.*, 2017, **7**, 24030-24039.
52. D. Yun, H. O. Kim, H. Y. Son, Y. Choi, I. Noh, J. W. Lim, J. Kim, H. Chun, G. Park, D. K. Lee and S. I. Jang, *J. Mater. Chem. B*, 2017, **5**, 6317-6324.
53. W. Yang, Q. Hu, Y. Xu, H. Liu and L. Zhong, *Mater. Sci. Eng. C*, 2018, **89**, 328-335.
54. K. K. N. Frese, A.; Cook, N.; Bapiro, T. E.; Lolkema, M. P.; Jodrell, D. I.; Tuveson, D. A., *Cancer Discov.*, 2012, **2**, 260-269.
55. H. Meng, M. Wang, H. Liu, X. Liu, A. Situ, B. Wu, Z. Ji, C. H. Chang and A. E. Nel, *ACS Nano*, 2015, **9**, 3540-3557.
56. I. Noh, H.-O. Kim, J. Choi, Y. Choi, D. K. Lee, Y.-M. Huh and S. Haam, *Biomaterials*, 2015, **53**, 763-774.
57. N. Awasthi, C. H. Zhang, A. M. Schwarz, S. Hinz, C. G. Wang, N. S. Williams, M. A. Schwarz and R. E. Schwarz, *Carcinogenesis*, 2013, **34**, 2361-2369.
58. N. Larson, J. Yang, A. Ray, D. L. Cheney, H. Ghandehari and J. Kopeček, *Int. J. Pharm.*, 2013, **454**, 435-443.
59. Y. Yu, C.-K. Chen, W.-C. Law, E. Weinheimer, S. Sengupta, P. N. Prasad and C. Cheng, *Biomacromolecules*, 2014, **15**, 524-532.
60. C. Drappier, A. L. Wirocius, K. Bathany, E. Ibarboure, O. Condassamy, E. Garanger and S. Lecommandoux, *Polym. Chem.*, 2013, **4**, 2011-2018.
61. K. Gu, J. Onorato, S. S. Xiao, C. K. Luscombe and Y.-L. Loo, *Chem. Mater.*, 2018, **30**, 570-576.
62. D. Chitkara, A. Mittal, S. W. Behrman, N. Kumar and R. I. Mahato, *Bioconjugate Chem.*, 2013, **24**, 1161-1173.
63. N. Li, H. Cai, L. Jiang, J. N. Hu, A. Bains, J. Hu, Q. Y. Gong, K. Luo and Z. W. Gu, *ACS Appl. Mater. Inter.*, 2017, **9**, 6865-6877.